IOP PUBLISHING JOURNAL OF PHYSICS: CONDENSED MATTER

J. Phys.: Condens. Matter 20 (2008) 045212 (7pp) doi:10.1088/0953-8984/20/04/045212

Evolution of the electronic structure and physical properties of Fe_2MeAl (Me = Ti, V, Cr) Heusler alloys

E Shreder[1], S V Streltsov[1], A Svyazhin[1], A Makhnev[1], V V Marchenkov[1], A Lukoyanov[2] and H W Weber[3]

[1] Institute of Metal Physics, S Kovalevskaya Street, 18, 620041 Ekaterinburg, Russia
[2] Ural State Technical University-UPI, Mira Street, 19, 620002 Ekaterinburg, Russia
[3] Atomic Institute of the Austrian Universities, Stadionallee, 2, 1020 Vienna, Austria

E-mail: shreder@imp.uran.ru

Received 19 September 2007, in final form 13 November 2007
Published 8 January 2008
Online at stacks.iop.org/JPhysCM/20/045212

Abstract

We present the results of experiments on the optical, electrical and magnetic properties and electronic structure and optical spectrum calculations of the Heusler alloys Fe_2TiAl, Fe_2VAl and Fe_2CrAl. We find that the drastic transformation of the band spectrum, especially near the Fermi level, when replacing the Me element (Me = Ti, V, Cr), is accompanied by a significant change in the electrical and optical properties. The electrical and optical properties of Fe_2TiAl are typical for metals. The abnormal behavior of the electrical resistivity and the optical properties in the infrared range for Fe_2VAl and Fe_2CrAl are determined by electronic states at the Fermi level. Both the optical spectroscopic measurements and the theoretical calculations demonstrate the presence of low-energy gaps in the band spectrum of the Heusler alloys. In addition, we demonstrate that the formation of Fe clusters may be responsible for the large enhancement of the total magnetic moment in Fe_2CrAl.

(Some figures in this article are in colour only in the electronic version)

1. Introduction

Heusler alloys X_2MeZ (X and Me are transition elements, Z is an element of the III–V subgroups) have been of considerable scientific interest for a long time. Nowadays the Heusler alloys are among the most investigated systems because of their unusual physical properties and possible practical applications. In particular, they are regarded as potential magnetooptical recording media [1] and materials for thermoelectric applications [2]. Some of them were theoretically predicted to be in a half-metallic state [3, 4]. The main feature of the electronic structure of half-metallic ferromagnets (HMF) is the presence of an energy gap at the Fermi level in one spin subband, and the metallic character of the density of states (DOS) in the other subband. This leads to 100% spin polarization of charge carriers. Such alloys are being intensively investigated as potential materials for spintronic devices [5].

During the last few years a lot of attention has been paid to the Fe_2MeAl Heusler alloys, where Me is a 3d transition metal (Me = Ti, V, Cr, Mn, Ni). The main peculiarity of the Fe_2VAl alloy is the formation of a hybridization pseudogap at the Fermi level in both spin subbands [6–8]. The presence of such a pseudogap is responsible for the anomalies observed in the transport properties of the Fe_2VAl. While it is natural to expect metallic behavior of the physical properties in these alloys, considering the metallic components, the Fe_2VAl compound demonstrates semiconductor-like behavior of the electrical resistivity, along with a very high value of the residual resistivity [9]. The electronic specific heat coefficient γ was found to approach $\gamma = 14\ \mathrm{mJ\,mol^{-1}\,K^{-2}}$. It was assumed initially that Fe_2VAl was a heavy-fermion system with an electronic effective mass 20–70 times greater than theoretically expected [9]. This disagreement was partly explained by the fact that the samples were subjected to different heat treatments, because the heat treatment influences the electronic heat capacity coefficient to a great extent. Later it was noticed that the specific heat and the electrical and magnetic properties of the alloy strongly depended on the melting method and on the subsequent heat treatment [10]. For instance, the residual

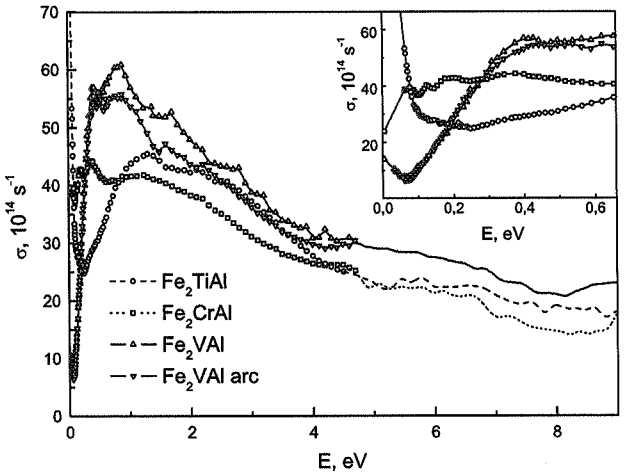

Figure 1. Optical conductivity dispersion of σ. The inset gives details of the optical conductivity in the low-energy range. The static conductivity σ_{st} (293 K) obtained from the $\rho(T)$ measurements is shown on the ordinate.

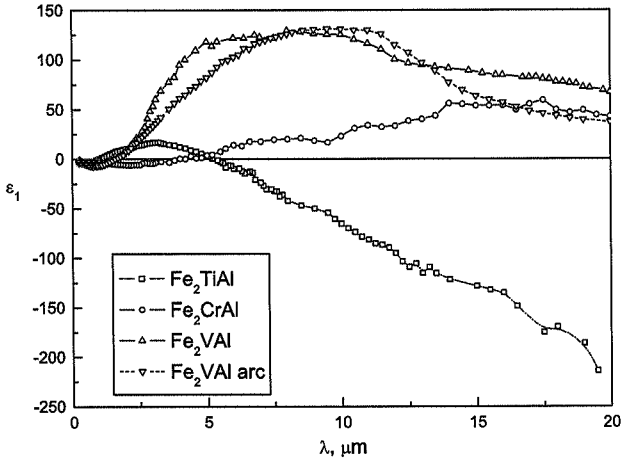

Figure 2. Dispersion of the real part of the dielectric constant ε_1.

resistivity of arc-melted samples, annealed at 1273 K and then slowly furnace cooled, is much less than that of samples annealed at lower temperatures or of quenched samples. The lowest value of the residual resistivity was found in an alloy melted in an induction furnace [11]. This can provides evidence for a change in the degree of order in the alloy. Together with the anomalously low concentration of charge carriers, this leads to an unusual resistivity behavior. Recently, we obtained a specimen of this alloy that possesses, to our knowledge, the lowest electronic heat capacity coefficient [12]. We have also discovered a contribution of ferromagnetic clusters to low-temperature heat capacity in Fe_2VAl alloy. The dependence of electrical resistivity, magnetic properties and electronic heat capacity on number and volume of the clusters was investigated as well [12].

The authors of [13] assumed that the Fermi level moved out of the pseudogap when replacing one d element by another, and that this should result in the disappearance of anomalies in the transport properties. Indeed, band structure calculations show such a transformation of the band spectrum. The experimental study of the transport properties of the stoichiometric Fe_2TiAl alloy confirmed these values and the resistivity behavior [14, 15]. The Fe_2CrAl alloy has a negative semiconductor-like temperature dependence of the resistivity $\rho(T)$ (temperature coefficient $b = 1/\rho * d\rho/dT < 0$) in the whole temperature range and does not show any features at the magnetic transition point, $T_C = 246$ K [16, 17].

To investigate the influence of the Me constituent in the Fe_2MeAl series on the physical properties and the electronic structure, we studied these alloys, where Me = Ti, V, Cr, by *ab initio* band structure calculations as well as by optical, magnetic and electrical measurements on these compounds. The influence of the heat treatment on the optical and electrical properties of Fe_2VAl was also investigated, in order to distinguish between the electronic structure features and those related to sample preparation.

2. Experimental results

The samples Fe_2TiAl, Fe_2VAl and Fe_2CrAl were melted in an induction furnace in an atmosphere of purified argon. The samples were remelted three times to ensure uniform constituent mixing. The sample of Fe_2TiAl was annealed for 48 h at 800 K in Ar atmosphere followed by cooling at 100 °C h^{-1}. The second sample Fe_2VAl was melted and remelted three times in an arc furnace in an atmosphere of purified helium. X-ray diffraction confirmed the formation of the $L2_1$ structure: the (111) and (200) superlattice peaks are present. The lattice parameters a are 0.5858 nm for Fe_2TiAl, 0.5761 nm for Fe_2VAl and 0.5811 nm for Fe_2CrAl. A small amount of the Fe_2Ti phase with $C14$ structure is present in the Fe_2TiAl sample. Note that the presence of an additional phase was also mentioned in [14, 18]. Smooth surfaces for the optical investigations were obtained by means of mechanical grinding with B-micropowders and subsequent polishing with chromium oxide. The dispersions of the real $\varepsilon_1(\omega)$ and imaginary $\varepsilon_2(\omega)$ parts of the complex dielectric function, and the optical conductivity $\sigma(\omega)$ (where ω is the optical wave cyclic frequency) were measured by the ellipsometric Beattie technique in the spectrum range $\lambda = (0.25\text{–}20)$ μm at room temperature. In the range $\lambda = (0.125\text{–}0.25)$ μm the optical conductivity $\sigma(\omega)$ was obtained from the measured reflectivity spectrum $R(\omega)$ using the Kramers–Kronig relations. Figures 1 and 2 show the optical conductivity σ and the real part of the complex dielectric function ε_1. The magnetic measurements were carried out using a SQUID magnetometer (Quantum Design) at $T = (4\text{–}293)$ K. The resistivity $\rho(T)$ was measured in the temperature range from 4.2 to 400 K.

2.1. Magnetic properties

Measurements of the temperature and field dependence of the magnetization and the *ac* susceptibility (figure 3) show that Fe_2CrAl is a ferromagnet with $T_C = 246$ K. Fe_2VAl and Fe_2TiAl exhibit spontaneous magnetization at 4 K. The *ac* susceptibility exhibits peaks at $T = 7$ K for Fe_2VAl and $T = 108$ K for Fe_2TiAl. These peculiarities indicate that

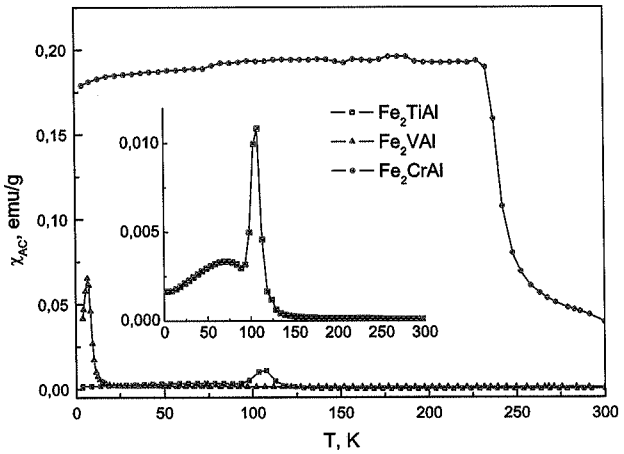

Figure 3. Temperature dependence of the *ac* susceptibility.

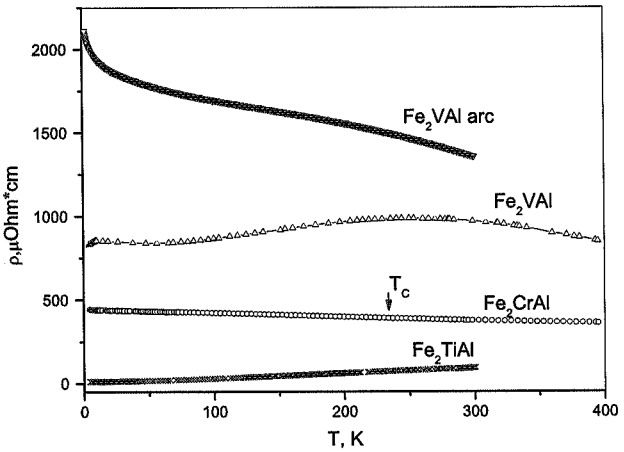

Figure 4. Temperature dependence of the electrical resistivity $\rho(T)$.

these alloys are ferrimagnets with small differences between magnetic moments ↑ and ↓ (about 0.1 μ_B). The Fe_2VAl band structure calculations showed that this alloy was non-magnetic. However, the real samples can have antisite defects playing the determining role in the formation of the magnetic state. The Fe atom in the V position may be surrounded by eight Fe atoms (clustering) and may possess a magnetic moment of about 2.2 μ_B resembling Fe_3Al.

There is no unanimous opinion on the magnetic state of Fe_2TiAl. Some authors consider this alloy to be a paramagnet [18]. Others [19] suggest that this compound is either a Pauli ferromagnet or an antiferromagnet and the ferromagnetic contribution originates from ferromagnetic inhomogeneities because of small deviations from the perfect $L2_1$ type atomic ordering. The presence of antiferromagnetic Fe_2Ti ($T_N = 300$ K) is mentioned in these papers.

2.2. Electrical properties

The study of the magnetic properties of the alloys has revealed the presence of magnetic transitions. Therefore, the appearance of peculiarities in the $\rho(T)$ curves is to be expected at the magnetic transition temperatures. Figure 4 shows the temperature dependence of the electrical resistivity. The resistivity of Fe_2TiAl is of metallic character with a residual resistivity of 12 $\mu\Omega$ cm and does not show any peculiarities at the magnetic transition point. This is in an agreement with previously reported data [14, 15]. Fe_2VAl shows abnormal electrical resistivity behavior. There are regions of positive and negative temperature coefficient b in the resistivity of the sample melted in an induction furnace, and only a semiconductor-like behavior for the arc-melted sample. A similar temperature dependence of the resistivity in Fe_2VAl (semiconductor-like or positive and negative temperature coefficient) was reported in [9, 10] as a result of the heat treatment. Fe_2CrAl has a negative semiconductor-like temperature dependence ($b = -0.22$) of the resistivity $\rho(T)$ with a linear character in a whole range of temperatures investigated and does not show any features at the point of magnetic transition (figure 4) [16].

2.3. Optical properties

The optical conductivity of usual metals and metallic alloys is a superposition of intra- and interband electron transitions. The intraband absorption is proportional to $1/\omega^2$ (a Drude-type growth) and plays a significant role in the low-energy infrared (IR) spectral range. The optical measurements in the IR-range enable us to determine the magnitudes of low-energy gaps in the energy-band spectrum. The optical criterion for a metallic type of band spectrum is a negative value of the real part of the dielectric constant in $\varepsilon_1(\omega)$ in the low-frequency range and a Drude-type growth of $\sigma(\omega)$ at $\omega \to 0$.

The optical conductivity σ is shown in figure 1. The inset shows details at the low-energy range. The room temperature values of the static conductivity σ_{dc}, which is the limit of the optical conductivity at $\omega \to 0$, obtained from the measurements of $\rho(T)$ are shown on the ordinate for Fe_2VAl, Fe_2CrAl. For Fe_2TiAl σ_{dc} is equal to 130×10^{14} s^{-1}. Our measurements clearly show the changes in the optical spectra upon substituting one Me element by another, especially in the IR-range.

According to figure 1, the optical conductivity curves of both Fe_2VAl samples are quite similar. Hence, we conclude that the main features of the optical conductivity spectrum are dominated by the electronic structure, and, in contrast to the electrical properties, depend on the heat treatment only slightly. We observe interband transitions of the electrons at photon energies $E > 0.1$ eV that form an intense interband absorption band with a maximum value of the conductivity $\sigma(\omega) \sim 60 \times 10^{14}$ s^{-1} at 0.9 eV. We suppose that the sharp absorption edge is the beginning of interband transitions across a gap and estimate its width to be 0.1 eV. Three weak inflections at 0.11, 0.21 and 0.25 eV as well as a double maximum at 0.41 and 0.50 eV and peaks at 0.9 and 1.7 eV are found in the $\sigma(\omega)$ dispersion curve. At least three weak absorption peaks at 0.035, 0.042 and 0.06 eV (see the inset in figure 1) and inflections at 0.038 and 0.052 eV, located slightly below the edge of the absorption fundamental band, are observed. These peaks are masked by the intraband contribution.

The main feature in the optical spectrum of Fe_2CrAl is the high level of the interband absorption ($\sigma(\omega) \sim 40 \times 10^{14}$ s^{-1})

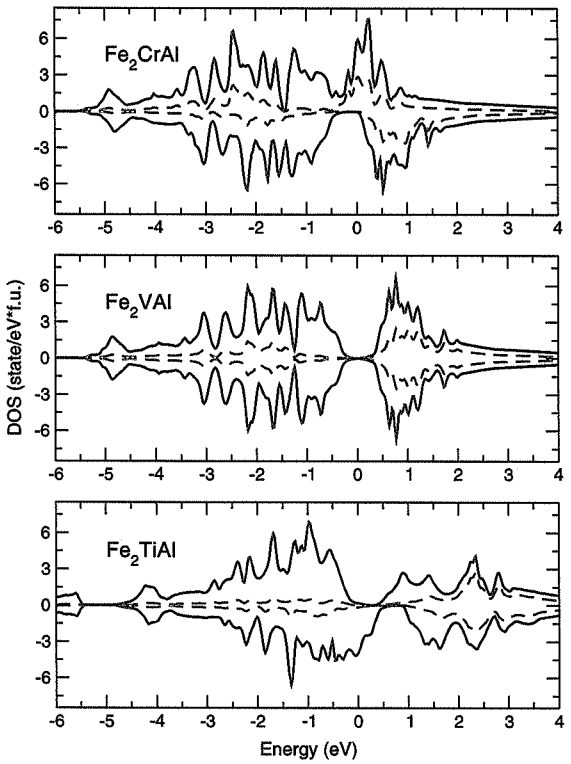

Figure 5. Density of states (DOS) for Fe_2TiAl, Fe_2VAl and Fe_2CrAl. The positive (negative) ordinates correspond to the spin majority (minority) DOS. The Fermi level is located at zero energy.

and the absence of intraband absorption in the IR-range up to the low-energy boundary 0.06 eV. The interband absorption has peaks at energies 0.067, 0.08, 0.124, 0.2, 0.38 eV, a wide maximum with a top at 1.24 eV, and then decreases to 8.2 eV. We note a peak at $E \sim 4.5$ eV and a 'shoulder' at (5–7) eV.

2.3.1. Intraband absorption. The intraband absorption is determined by the parameters of the conduction electrons, relaxation Γ and plasma frequencies Ω. The squared plasma frequency Ω^2 is proportional to the Fermi velocity of the carriers and to the effective concentration of the free carriers N_{eff}. Dominant intraband absorption is indicated by negative values of ε_1 in the IR-range. Figure 2 presents the dispersion curves of ε_1. The Drude-type growth of the optical conductivity and negative values of ε_1 in the IR-range, typical for optical spectra of metals, are found only for Fe_2TiAl. An abnormal behavior of $\sigma(\omega)$ and $\varepsilon_1(\omega)$ is observed for Fe_2CrAl and Fe_2VAl. For Fe_2VAl, the Drude-type growth is very weak and observed at energies below $E \sim 0.06$ eV. A linearization of the $1/(1-\varepsilon_1) = f(\omega^2)$ dependence results in the following estimates for $\hbar\Omega$: 0.104 eV for Fe_2VAl and 3.5 eV for Fe_2TiAl (see table 1). The effective concentration of free carriers N_{eff} derived from the IR-range of $\sigma(\omega)$, is found to be 10^{19} and 10^{21} cm^{-3} for Fe_2VAl and Fe_2TiAl, respectively.

For Fe_2CrAl, the most interesting feature in the optical spectrum is the absence of the Drude-type growth and the high level of interband absorption of $\sigma(\omega) \sim 40 \times 10^{14}$ s^{-1} in the IR-range up to the low-energy boundary. The absence of

Table 1. Calculated and experimental values of magnetic moment and plasma frequency.

Alloy	μ_{calc} (μ_B/f.u.)	μ_{exp} (μ_B/f.u.)	Ω_{calc} (eV)	Ω_{exp} (eV)
Fe_2TiAl	0.88	0.1	5.4	3.5
Fe_2VAl	0	0	1.5	0.1
Fe_2CrAl	1.0	1.78	2.5	—

the Drude-type growth makes the determination of Γ and Ω impossible. In the low-frequency limit $\omega \to 0$, the value of the optical conductivity should be equal to the value of the static conductivity $\sigma_{\text{dc}} = 24 \times 10^{14}$ s^{-1}.

There is a correlation between the electrical and the optical properties of the alloys. The increase in N_{eff} is accompanied by an essential growth of the conductivity. The $\rho(T)$ curve for Fe_2TiAl demonstrates the metallic character of conductivity in the temperature range (4.2–400) K (figure 4). For Fe_2VAl, the resistivity is characterized by relatively high values (750–850) $\mu\Omega$ cm and regions of positive and negative temperature coefficient $b = 1/\rho * d\rho/dT$ [11]. Fe_2CrAl shows a negative temperature dependence of the resistivity $\rho(T)$ with a linear character ($b = -0.22$) in the temperature range (4.2–400) K, and no features are observed at the magnetic transition point [16].

3. Band structure and optical spectrum calculations

3.1. Band structure calculations

Ab initio band structure calculations in the generalized gradient approximation (GGA) were carried out in order to understand the features of the optical conductivity spectra and the magnetic properties of the Fe_2MeAl alloys. The calculation was done in the framework of the full-potential linearized augmented plane-wave (FP-LAPW) method using the Wien2k code [20]. We used a 1000 k-points mesh in the process of self-consistency and 30 000 k-points for calculations of the optical properties. The non-overlapping muffin-tin (MT) sphere radii of 2.35 au for V, Cr, Ti, (2.2–2.25) au for Al and (2.3–2.4) au for Fe atoms were used. The expansion in the spherical harmonics of the radial wavefunctions was taken up to $l = 10$. The value of $R_{\text{MT}}^{\text{min}} K^{\text{max}}$, where $R_{\text{MT}}^{\text{min}}$ is the minimal MT radius and K^{max} is the plane-wave cut-off, was set to 7.0. The optical properties were computed using an explicit evaluation of the momentum matrix elements [21]. We used 0.05 eV broadening for the interband spectra calculations.

The total density of states for Fe_2VAl is shown in the middle panel of figure 5. Its character is quite unusual for an alloy, since the valence and the conduction bands are separated by a pseudogap. In accordance with [6, 7], the top of the valence band is formed mostly by Fe-t_{2g} states, while the bottom of the conduction band predominantly has V-3d and Fe-e_g characters (note that there are two Fe atoms per f.u. (formula unit)). This structure of the DOS turns out to be related to the magnetic properties of the Fe_2MeAl alloys.

The interchange of V and Ti, which has one electron less, does not lead to a significant reconstruction of the electronic structure, but rather to a rigid shift of the Fermi level to the

valence band. In Fe_2TiAl, the Fe-t_{2g} partial DOS runs over the Fermi level. This results in a Stoner instability in the Fe band and the formation of long-range magnetic order. The magnetic moment indeed develops mostly at Fe ions: $\mu_{Fe} = 1.07\ \mu_B$/f.u. (total moment $\mu = 0.88\ \mu_B$/f.u.). Quite similar values were obtained in other band structure studies [15].

It is rather intriguing that this natural picture does not correspond to the experimental findings. According to [1] and our present measurements, the saturation magnetization in Fe_2TiAl is $\sim 0.1\ \mu_B$. From a theoretical point of view, it would be very surprising if disorder effects led to the disappearance of the magnetic moment in the system. On the contrary, it rather results in the formation of magnetic clusters. One would also speculate that Fe_2TiAl is near the metamagnetic quantum critical point and that the strong spin fluctuations, which are not considered on the local spin density approximation (LSDA) or GGA level, may suppress the magnetic instability in the material. Moruzzi and Marcus found that LSDA indeed significantly overestimated the tendency to magnetism in FeAl and FeV and even resulted in an incorrect magnetic state for these alloys [22]. This failure seems to arise from the LSDA, which is based on the assumption that the electronic gas is uniform. Such a state is far from any magnetic critical points at densities relevant for the solids. Guo and co-authors used LSDA for the investigation of electronic properties of Fe_2VAl and argued that large enhancement of electronic specific heat is due magnetic fluctuations [23]. Thus, the origin of the strong suppression of the magnetic moment in Fe_2TiAl may also be related to spin fluctuations. In order to check this assumption, further theoretical investigations beyond the framework of the LSDA or GGA formalism are required, as was done for instance in [24].

The addition of an extra electron, by the change from V to Cr in Fe_2MeAl, again leads to a shift of the Fermi level and to a partial occupation of the conduction band [25]. But in this case the Fermi level gets to a region, where the DOS has mostly Me-3d character. As a result, the magnetic moment in Fe_2CrAl develops at the Cr ions: $\mu_{Cr} = 1.1\ \mu_B$/f.u. (total moment $\mu = 1.0\ \mu_B$/f.u.). This also differs from the experimental value of 1.67 μ_B [1] or 1.78 μ_B [16], but can be explained by the presence of intrinsic disorder or defects in Heusler alloys. Indeed, considering the FeAl alloy, Kulikov and co-workers showed that antisite defects and vacancies may considerably increase the local magnetic moments [26].

Since the difference between the experimental value and calculated moment for the fully ordered pattern is large, one may assume that there is not simply a chaotic distribution of antisite defects in Fe_2CrAl, but rather a kind of clustering. If true, such clusters should be made out of Fe ions. Indeed, metallic bulk Fe is ferromagnetic (FM) with $\mu = 2.2\ \mu_B$/f.u. [27], while bulk Cr is antiferromagnetic (AFM) with $\mu = 0.6\ \mu_B$/f.u. [28] and hence Cr clusters may only reduce the total magnetization of Fe_2CrAl. Keeping the same chemical composition, we may construct Fe clusters interchanging Fe atoms with Al or Cr ones. The replacement of Al on Fe is preferable, since in this situation we do not break the already FM Cr lattice.

In order to check the possibility of reaching large magnetic moment in Fe_2CrAl forming an Fe cluster, we produced additional super-cell calculations in the framework of the linearized muffin-tin orbitals (LMTO) method, realized in the Stuttgart TB-LMTO-47 computer code [29]. This method is much less time-consuming than LAPW since it uses atomic-like wavefunction in the basis set. We used the $4 \times 4 \times 4$ super-cell. The integration in the Brillouin zone was performed by a direct summation using the Methfessel–Paxton algorithm [30], since the tetrahedral method used for the large super-cells leads to charge fluctuation, due to the presence of many nearly degenerate bands in the vicinity of the Fermi level. The Methfessel–Paxton width parameter was chosen to be 0.05 eV and we used a mesh of 64 k-points (which is big enough for the large super-cell) in the irreducible part of the Brillouin zone for the calculation.

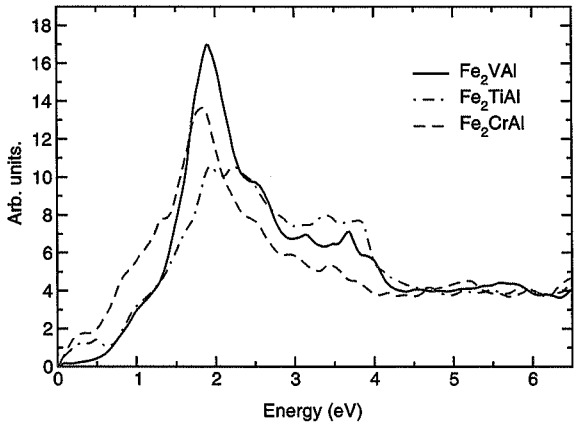

Figure 6. Interband part of the calculated optical conductivity. Spin majority and spin minority are summed up.

We found that the interchange of 6% of the atoms according to the calculations presented above does not lead to sufficient enhancement of the total magnetic moment, since a large number of Fe atoms turn out to be polarized in the opposite direction with respect to Cr atoms trying to compensate Cr field. Further increase of the number of replaced atoms up to 12% results in a total magnetic moment of 1.67 μ_B/f.u., which is in a good agreement with magnetic measurements [1, 16]. The largest magnetic moment 2.53 μ_B was found in the center of an Fe cluster. The average magnetic moments, taking into account the signs, are $-0.17\ \mu_B$ per Cr and 1.91 μ_B per Fe atoms.

In addition to this configuration, we tried to make Fe clusters by replacing Cr and Fe atoms. For 6% of interchanged atoms the net magnetic moment was found to be nearly zero, while for the case of 12% it is $\sim 1.01\ \mu_B$.

3.2. Optical spectrum calculations

The calculated optical conductivity for the fully ordered pattern obtained within the LAPW method is shown in figure 6. While the quantitative behavior of our experimental (figure 1) and theoretical (figure 6) curves is rather similar, it should be noted that the calculated graphs are shifted by ~ 1 eV to higher energies for all of the alloys. This is similar to other half-metallic ferromagnet systems, e.g. CrO_2, where the frequencies of the main spectral features in the optical

conductivity calculated within the density functional theory, are systematically overestimated by ~10–20% [31]. The quantitative discrepancy is clearly larger in the Heusler alloys because of the overestimation of the value of the pseudogap. This may be due to the deficiency of GGA method (absence of the electronic correlations) or because of the disorder effect discussed in the previous section (impurity states). Clustering of some sort of atoms or the presence of the antisite defects leads to the formation of in-(pseudo)gap states. It was argued in [32] that such impurity states may serve as an origin for the heavy-fermion like behavior in Fe_2VAl. In addition, based on the thorough analysis of the temperature dependence of resistivity, Hall effect and photoemission data, the authors of [33] proposed that the Fermi level in Fe_2VAl may be shifted from the middle of the pseudogap (as obtained in any band structure calculation [6, 7]) to the sharply rising portion of the valence band.

Our calculations for the fully ordered pattern reproduces the change of the optical spectra with the change of the Me element (Cr, V, Ti). The transitions between 3d states of V and Fe across the pseudogap result in the formation of the prominent peak at ~1.8 eV in the calculated interband optical spectra of Fe_2VAl. As described above and clearly seen in figure 5, substitution of V by Cr (Ti) leads to such a shift of the band structure that the Fermi level remains in the pseudogap only for one of the spin channels. Therefore, the position of this peak is almost the same for Fe_2CrAl and Fe_2TiAl, but the intensity is suppressed compared to Fe_2VAl. Similar changes are observed in the experimental graphs. However, the fine structure of the optical excitations near 1.8 eV in the calculated and near 1 eV in the experimental spectra is rather different for these three alloys. Smearing the pseudogap in the spin-up channel of Fe_2CrAl results in the formation of the 'shoulder' to the left of the main peak. The larger spread of empty states in Fe_2TiAl leads to the appearance of a more pronounced right 'shoulder' in Fe_2TiAl compared to Fe_2CrAl.

The intraband contributions to the optical spectra are found to be rather different for all three materials (see table 1). The presence of the pseudogap significantly suppresses the value of the plasma frequency Ω in Fe_2VAl. The shift of the Fermi level and its removal from the pseudogap in the Cr and Ti based alloys lead to an increase of the plasma frequency. Note that the increase of Ω is much larger for Fe_2TiAl.

The reason can be found from calculations of the partial contributions to the plasma frequency. Besides a hardly analyzable difference in the band slope at the Fermi energy (which defines the Fermi velocity and therefore Ω) the character of the electronic states forming the Fermi surface turns out to be important. As one can see from figure 5 these states have mostly Cr character for Fe_2CrAl and Fe for Fe_2TiAl. But there are two non-equivalent positions of Fe atoms in the unit cell. This results in doubling the number of sheets of the Fermi surface and Ω in Fe_2TiAl.

4. Conclusions

We find a drastic transformation of the band spectrum, especially near the Fermi level, when one Me element (Me = Ti, V, Cr) replaces another. These changes are closely related to the magnetic properties of the Fe_2MeAl alloys and accompanied by a drastic change in the electrical and the optical properties of these materials. Fe_2TiAl shows electrical and optical properties, which are typical for metals. The abnormal behavior of the electrical resistivity and the optical properties in the IR-range, found in Fe_2VAl, is determined by the electronic states at the Fermi level. The calculated magnetic moments for the fully ordered patterns of Fe_2CrAl and Fe_2TiAl are far from those obtained experimentally. We show that the formation of Fe clusters with the replacement of 12% of atoms may explain the increase of the total magnetic moment in Fe_2CrAl. The possible role of spin fluctuations for the Fe_2MeAl series is also indicated. The computed optical spectra reproduce the main spectral features, but systematically overestimate the positions of the main spectral peaks.

At present, half-metallic ferromagnetic materials are of great interest for spintronics as an injector of spin-polarized electrons. Therefore, the results of the present work provide a starting point for further studies. With doping, the position of the Fermi level in $Fe_{2-x}Cr_{1+x}Al$ can be fine-tuned. In particular, a direct investigation of disorder effects in Heusler alloys seems to be challenging.

Acknowledgments

We wish to thank Igor Mazin for fruitful discussions about the possible role of defects in Heusler alloys and Vladimir Anisimov for his helpful suggestions. This work is supported by the Russian Foundation for Basic Research (project 05-02-16930), INTAS via YS fellowship 05-109-4727, the Civil Research and Development Foundation together with the Russian Ministry of Science and Education through grant Y4-P-05-15, the Dynasty Foundation and International Center for Fundamental Physics in Moscow, the Russian president grant for young scientists MK-1184.2007.2 and the Austrian Academy of Sciences.

References

[1] Buschow K H J, van Engen P G and Jongenbreur R 1983 *J. Magn. Magn. Mater.* **38** 1–22
[2] Lue C S and Kuo Y-K 2002 *Phys. Rev.* B **66** 085121
[3] De Groot R A, Muller F M, Mueller P G, van Engen P G and Bushow K H J 1983 *Phys. Rev. Lett.* **50** 2024–7
[4] Fujii S, Sugimura S, Ishida S and Asano S 1990 *J. Phys.: Condens. Matter* **2** 8583–9
[5] Irkhin V and Katsnelson M 1994 *Phys.—Usp.* **37** 659–76
[6] Singh D and Mazin I 1998 *Phys. Rev.* B **57** 14352–6
[7] Ruben W and Pickett W 1998 *Phys. Rev.* B **58** 6855–61
[8] Bansil A, Kaprzyk S, Mijnarends P and Tobola J 1999 *Phys. Rev.* B **60** 13396–412
[9] Nishino Y, Kato M, Asano S, Soda K, Hayasaki M and Mizutani U 1997 *Phys. Rev. Lett.* **79** 1909–12
[10] Matsushita A and Yamada Y 1999 *J. Magn. Magn. Mater.* **196/197** 669–70
[11] Shreder E, Kirillova M, Makhnev A and Dyakina V 2002 *Phys. Met. Metallogr.* **93** 152–8
[12] Podgornykh S M, Svyazhin A D, Shreder E I, Marchenkov V V and Dyakina V P 2007 *JETF* **105** 42–5

[13] Botton G A, Nishino Y and Humphreys C J 2000 *Intermetallics* **8** 1209–14
[14] Kato M *et al* 2000 *J. Phys.: Condens. Matter* **12** 9153–62
[15] Slebarski A, Goraus J, Deniszczyk J and Skoczen L 2006 *J. Phys.: Condens. Matter* **18** 10319–34
[16] Shreder E *et al* 2005 *Phys. Met. Metallogr.* **99** 393–400
[17] Zhang M, Bruck E H, de Boer F R and Wu G H 2004 *J. Magn. Magn. Mater.* **283** 409–14
[18] Okpalugo D E, Booth J G and Faunce C A 1985 *J. Phys. F: Met. Phys.* **15** 681–92
[19] Buschow K H J and van Engen P G 1981 *J. Magn. Magn. Mater.* **25** 90–6
[20] Blaha P *et al* 2001 *WIEN2k, An Augmented Plane Wave + Local Orbitals Program for Calculating Crystal Properties* Karlheinz Schwarz Techn. Universität Wien Austria
[21] Ambrosch-Draxl C and Sofo J O 2006 *Comput. Phys. Commun.* **175** 1–14
[22] Moruzzi V L and Marcus P M 1993 *Phys. Rev.* B **47** 7878–84
[23] Guo G Y, Botton G A and Nishino Y 1998 *J. Phys.: Condens. Matter* **10** L119–26
[24] Mazin I I, Singh D J and Aguayo A 2003 *Proc. NATO ARW on Physics of Spin in Solids: Materials, Methods and Applications* ed S Halilov (Dordrecht: Kluwer) (*Preprint* cond-mat0401563)
[25] Shreder E, Svyazhin A and Streltsov S 2005 *Phys. Met. Metall.* **100** (Suppl. 1) S116–20
[26] Kulikov N I, Postnikov A V, Borstel G and Braun J 1999 *Phys. Rev.* B **59** 6824–33
[27] Kittel C 1986 *Introduction to Solid State Physics* 6th edn (New York: Wiley)
[28] Bolef D I and de Klerk J 1963 *Phys. Rev.* **129** 1063–7
[29] Anderson O K and Jepsen O 1984 *Phys. Rev. Lett.* **53** 2571–4
[30] Methfessel M and Paxton A T 1989 *Phys. Rev.* B **40** 3616–21
[31] Mazin I I, Singh D J and Ambrosch-Draxl C 1999 *Phys. Rev.* B **59** 411–8
[32] Deniszczyk J and Borgiel W 2003 *Acta Phys. Pol.* B **34** 1257–60
[33] Okamura H *et al* 2000 *Phys. Rev. Lett.* **84** 3674–7